JOURNAL OF GEOPHYSICAL RESEARCH, VOL. 98, NO. A11, PAGES 19,049–19,063, NOVEMBER 1, 1993

Parametric Instabilities of Parallel-Propagating Alfvén Waves: Some Analytical Results

V. JAYANTI AND JOSEPH V. HOLLWEG

Physics Department and Institute for the Study of Earth, Oceans and Space, University of New Hampshire, Durham

We consider the stability of a circularly polarized Alfvén wave (the pump wave) which propagates parallel to the ambient magnetic field. Only parallel-propagating perturbations are considered, and we ignore dispersive effects due to the ion cyclotron frequency. The dissipationless MHD equations are used throughout; thus possibly important effects arising from Landau and transit time damping are omitted. We derive a series of analytical approximations to the dispersion relation using $A = (\Delta B/B_0)^2$ as a small expansion parameter; ΔB is the pump amplitude, and B_0 is the ambient magnetic field strength. We find that the plasma β (the square of the ratio of the sound speed to the Alfvén speed) plays a crucial role in determining the behavior of the parametric instabilities of the pump. If $0 < \beta < 1$ we find the familiar result that the pump decays into a forward propagating sound wave and a backward propagating Alfvén wave with maximum growth rate $\gamma_{max} \propto A^{1/2}$, but β cannot be too close to 0 or to 1. If $\beta \approx 1$, we find $\gamma_{max} \propto A^{3/4}$; if $\beta > 1$, we find $\gamma_{max} \propto A^{3/2}$, while if $\beta \approx 0$, we obtain $\gamma_{max} \propto A^{1/3}$; moreover, if $\beta \approx 0$ there is a nearly purely growing instability. In contrast to the familiar decay instability, for which the backward propagating Alfvén wave has lower frequency and wavenumber than the pump, we find that if $\beta \gtrsim 1$ the instability is really a beat instability which is dominated by a transverse wave which is forward propagating and has frequency and wavenumber which are nearly twice the pump values. Only the decay instability for $0 < \beta < 1$ can be regarded as producing two recognizable normal modes, namely, a sound wave and an Alfvén wave. We discuss how the different characteristics of the instabilities may affect the evolution of Alfvén waves in the solar wind. However, for a solar wind in which $\beta \approx 1$ the growth times of the instabilities are probably too long for these instabilities to have an appreciable effect inside 1 AU.

1. INTRODUCTION

A circularly polarized Alfvén wave propagating along the ambient magnetic field is an exact solution to the MHD equations, even when the wave amplitude is large [*Abraham-Shrauner and Feldman*, 1977; *Barnes and Hollweg*, 1974; *Barnes and Suffolk*, 1971]. However, *Galeev and Oraevskii* [1963] and *Sagdeev and Galeev* [1969] showed that the Alfvén wave is unstable: it can decay into a backward propagating Alfvén wave and a forward propagating sound wave. *Goldstein* [1978] and *Derby* [1978] derived the following dispersion relation for perturbations about a background consisting of the ambient magnetic field plus the circularly polarized "pump" Alfvén wave:

$$\{(x^2 - b^2y^2)(x - y)[(x + y)^2 - 4] - Ay^2(x^3 + x^2y + y - 3x)\}(x - y) = 0 \qquad (1)$$

where $x = \omega/\omega_0$, $y = k/k_0$, ω_0, and k_0 are the angular frequency and wavenumber of the pump wave, ω and k are the angular frequency and wavenumber of the plasma density perturbations (see *Jayanti and Hollweg* [1993] for a discussion of the importance of properly specifying the meanings of ω and k), $b = v_s/v_A$ is the ratio of the sound speed v_s to the Alfvén speed v_A, and $A = (\Delta B)^2/B_0^2$ is the square of the ratio of the pump wave amplitude ΔB to the ambient field strength B_0. Equation (1) is valid for a low-frequency pump wave with dispersive effects neglected; thus $\omega_0^2/k_0^2 = v_A^2$. Equation (1) is also valid only for the case where the pump wave and all perturbations propagate parallel or antiparallel to the ambient magnetic field. Finally, (1) has been derived from the MHD equations; collisionless effects such as Landau and transit time damping are therefore omitted. *Sakai and Sonnerup* [1983], *Terasawa et al.* [1986], *Longtin and Sonnerup* [1986], and *Wong and Goldstein* [1986] extended (1) to include dispersive effects which arise from the finite gyroperiod of a single massive ion, while *Viñas and Goldstein* [1991] consider perturbations which propagate at a nonzero angle to the ambient field. *Hollweg et al.* [1993] consider new instabilities which can arise in a plasma consisting of electrons, protons, and streaming alpha particles. In this paper we will consider only (1).

Equation (1) and its extensions have been considered numerically (see especially *Wong and Goldstein* [1986]), but surprisingly little attention has been given to analytical solutions. *Galeev and Oraevskii* [1963] considered a small-amplitude pump wave in a low-β plasma (where $\beta \equiv b^2$). They approximated the maximum growth rate γ for the decay instability as

$$\gamma_{max} \approx A^{1/2}\beta^{-1/4}\omega_0/2 \qquad (2)$$

Even though this equation is for a low-β plasma, it clearly fails as $\beta \to 0$. One of the goals of this paper is to provide an expression for γ_{max} which is valid for $\beta \approx 0$. However, we shall also consider approximate analytical solutions to (1) for a full range of values of β. For values of β between 0 and 1 we will obtain a generalization of (2) which reduces to (2) when $\beta \ll 1$. However, as $\beta \to 0$, we will find that a different approximation procedure is required and that $\gamma_{max} \propto A^{1/3}$, in contrast to the scaling $\gamma_{max} \propto A^{1/2}$ found for β between 0 and 1. We will also find that a different approximation scheme is required when $\beta \approx 1$; in that case we will find that $\gamma_{max} \propto A^{3/4}$. Finally, if β is greater than, but not close to 1, we will find that $\gamma_{max} \propto A^{3/2}$. We will also find that only when β is between 0 and 1, but not close to either limit, can the pump

Paper number 93JA02208.
0148-0227/93/93JA-02208$05.00

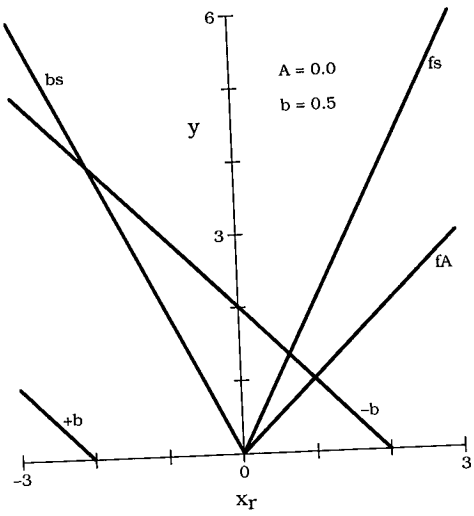

Fig. 1. Normalized wavenumber $y = k/k_0$ as function of normalized frequency $x = \omega/\omega_0$ for $A = 0.0$ and $b = 0.5$ ($\beta = 0.25$). The five roots are obtained from the exact dispersion relation (1); the sixth root $x = y$ is not shown. The notations *fs*, *fA*, and *bs* denote forward-sound, forward Alfvén, and backward sound waves, respectively. The notations $-b$ and $+b$ denote backward Alfvén waves involving (ω_-, k_-) and (ω_+, k_+), respectively.

wave be regarded as decaying into a forward propagating sound wave and a backward propagating Alfvén wave having lower frequency and wavenumber than the pump. In particular, when $\beta \gtrsim 1$, the instability is really a beat instability which is dominated by a forward propagating transverse wave having frequency and wavenumber which are nearly twice the pump values [cf. *Umeki and Terasawa*, 1992]. If $b \approx 0$, the instability produces a backward propagating wave which differs from the Alfvén wave in that it propagates slower than the Alfvén speed, and if $\beta \approx 0$ or $\beta > 1$, the sound wave is not involved in the instability.

These different characteristics of the instabilities may affect how Alfvén waves evolve in the solar wind. For example, the development of MHD turbulence in the solar wind is usually regarded as requiring both inward and outward propagating waves [*Dobrowolny et al.*, 1980], and the decay instability is a possible means of generating the inward waves from a field of outward propagating waves originating at the Sun. Similarly, the decay instability has been thought to provide a mechanism for explaining the increasing importance of inward propagating waves which is observed [*Marsch and Tu*, 1990; *Roberts et al.*, 1987] at greater heliocentric distances (see *Lou* [1993] for a different point of view). However, our results show that, in contrast to the decay instability, the beat instability which occurs when $\beta \gtrsim 1$ primarily produces outward propagating waves. Thus throughout much of the solar wind, where $\beta \gtrsim 1$, the parametric instabilities are a less attractive mechanism for initiating a turbulent cascade or for producing the observed inward waves. However, the beat instability may provide a direct mechanism for transferring energy to high wavenumbers, since the dominant unstable wave occurs roughly at $2k_0$.

At the outset, however, we should point out that our discussion will omit collisionless damping, which will be important in space plasmas such as the solar wind. All the parametric instabilities are mediated by density fluctuations, which are subject to ion Landau and transit time damping which are not included in the fluid model leading to (1). Collisionless damping will reduce the growth rates of the parametric instabilities [*Inhester*, 1990; *Terasawa et al.*, 1986], but the decay instability is known to survive even when the damping is strong. Thus our calculations are expected to be only qualitatively correct; we will discuss this issue further in section 8. However, our analysis will still be quantitatively useful when the damping is weak. We believe that our results will provide a useful analytical benchmark for interpreting MHD simulations of the parametric instabilities [e.g., *Agim et al.*, 1993; *Ghosh et al.*, 1993; *Ghosh and Goldstein*, 1993; *Hoshino and Goldstein*, 1989; *Umeki and Terasawa*, 1992] and for assessing the roles of kinetic effects in hybrid simulations [*Machida et al.*, 1987; *Terasawa et al.*, 1986] or in analytical treatments such as *Inhester*'s [1990].

Our analysis also omits any effects due to the ion cyclotron frequency. The modulational instability [e.g., *Longtin and Sonnerup*, 1986; *Machida et al.*, 1987] is therefore omitted, as is a less important beat instability [*Wong and Goldstein*, 1986]. Equation (1) therefore does not distinguish between right and left circularly polarized waves, and we do not recover the result that the decay instability has a somewhat faster growth rate when the pump wave is right-handed [*Wong and Goldstein*, 1986]. These effects may not be important for the low-frequency Alfvén waves in the solar wind, but their omission means that we can not treat ion-resonant waves upstream of the Earth's bow shock [see *Spangler*, 1992, and references therein].

2. Case $A = 0$

We will henceforth ignore the root $x = y$ which is always a factor of (1). In the limit of vanishingly small pump wave amplitude, $A \to 0$, the remaining roots of (1) are five straight lines in the x-y plane. Two of the roots are $x = by$ and $x = -by$. If we take $\omega_0 = k_0 v_A$ (a "forward propagating" pump), then these two roots correspond to forward propagating and backward propagating sound waves, respectively; they are denoted *fs* and *bs* (i.e., forward sound and backward sound) in Figure 1, which shows the five roots for $b = 1/2$ (only the first and second quadrants are shown, since $y(-x) = -y(x)$). The remaining three roots are Alfvén waves. Since ω and k have been defined to refer to the plasma density fluctuations and longitudinal (i.e., along $\mathbf{B}_0$) velocity fluctuations, the transverse velocity, and magnetic field fluctuations always have frequencies and wavenumbers given by $\omega_\pm = \omega_0 \pm \omega$ and $k_\pm = k_0 \pm k$. The root $x = y$ corresponds to a forward propagating Alfvén wave with $\omega_\pm/k_\pm = +v_A$; this root is denoted *fA* (i.e., forward-Alfvén) in Figure 1. The root $x + y = 2$ is a backward propagating Alfvén wave involving ω_- and k_-; i.e., $\omega_-/k_- = -v_A$; it is denoted $-b$ in Figure 1. Finally, the root $x + y = -2$ is a backward propagating Alfvén wave involving ω_+ and k_+; i.e., $\omega_+/k_+ = -v_A$; it is denoted $+b$ in Figure 1.

If $A \neq 0$, instabilities can occur in the first and third quadrants of Figure 1. The usual decay instability occurs near the intersection of the *fs* and $-b$ roots, and we consider that case in the next section.

3. Decay Instability: $0 < \beta < 1$

We consider the case of β between 0 and 1; however, we shall see below that β cannot be too close to 0 or 1. The soli

curves in Figure 2*a* show the roots of (1) for $A = 0.1$ and $b = 1/2$ (i.e., $\beta = 1/4$); we have taken y to be real, and Figure 2*a* displays the real part of x, denoted x_r. The roots corresponding to the lines fs, fA, and $-b$ in Figure 1 have been labeled accordingly. The existence of an instability is readily recognized by inspecting Figure 2*a*. The instability exists in the "gap" between the two hyperbolas. Above and below the gap, the hyperbolas give two real roots for x, for a given value of y. Within the gap, however, there is only one value of x_r for each value of y; this indicates that there are two complex conjugate roots for x, one of which is growing (unstable). In this case the gap represents the decay instability which involves a forward propagating sound wave and a backward propagating Alfvén wave; it occurs in the vicinity of the intersection of the fs and $-b$ roots. The solid curve in Figure 2*b* displays the positive imaginary part of x, denoted x_i; the values of x_i for the other root are the same as those displayed in Figure 2*b* but of opposite sign.

An analytical approximation for the unstable roots is obtained by expanding (1) around the point where the fs and $-b$ lines in Figure 1 intersect. This point has coordinates (x_s, y_s) given by

$$x_s = 2b/(1 + b) \tag{3a}$$

$$y_s = 2/(1 + b) \tag{3b}$$

The expansion point is indicated by the solid circle in Figure 2*a*. Thus we take $x = x_s + dx$, $y = y_s + dy$. We assume that A is small and of the order of ε and that dx and dy are of the order of $\varepsilon^{1/2}$. (The ordering of dx and dy is dictated by inspection of the mathematical form of (1).) The lowest-order terms in (1) are then of the order of ε. Setting these terms to zero gives the approximate dispersion relation,

$$8(1 - b)[4b(1 + b)^2(dy + dx)(b\ dy - dx) - A(1 - b)](1 + b)^{-4} + 0(\varepsilon^{3/2}) = 0 \tag{4}$$

The solutions to (4) are the dashed curves in Figure 2. Comparing the solid and dashed curves in Figure 2 shows that (4) gives a reasonable approximation to the full dispersion relation (1), except that the root $x = y$ is lost entirely. Thus we expect (4) to fail to describe the instability when the unstable roots to (4) overlap with the missing root $x \approx y$; this will tend to occur as $b \to 1$, since the fs and fA roots in Figure 1 then tend to overlap. Equation (4) also does not contain the root corresponding to backward propagating sound, $x \approx -by$. Thus we expect (4) to fail also when the unstable roots to (4) come close to the root for backward propagating sound; this will tend to occur as $b \to 0$.

According to (4) the maximum growth rate occurs when $dy = 0$:

$$\frac{\gamma_{max}}{\omega_0} \approx \frac{A^{1/2}(1 - b)^{1/2}}{2b^{1/2}(1 + b)} \tag{5}$$

which agrees with (2) for small b. Equation (4) also shows that the range of unstable wavenumbers is approximately

$$-\frac{A^{1/2}(1 - b)^{1/2}}{b^{1/2}(1 + b)^2} < dy < \frac{A^{1/2}(1 - b)^{1/2}}{b^{1/2}(1 + b)^2} \tag{6}$$

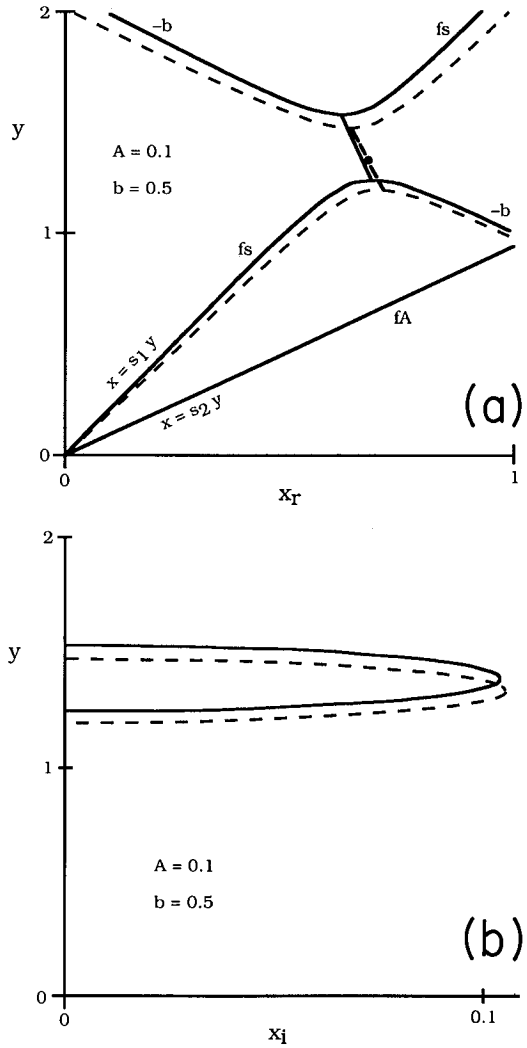

Fig. 2. The (*a*) real and (*b*) imaginary parts of x as functions of y for $A = 0.1$ and $b = 0.5$ ($\beta = 0.25$). The solid curves are the exact roots of (1); the dashed curves are obtained from approximation (4). The solid circle indicates the expansion point (x_s, y_s) given by (3).

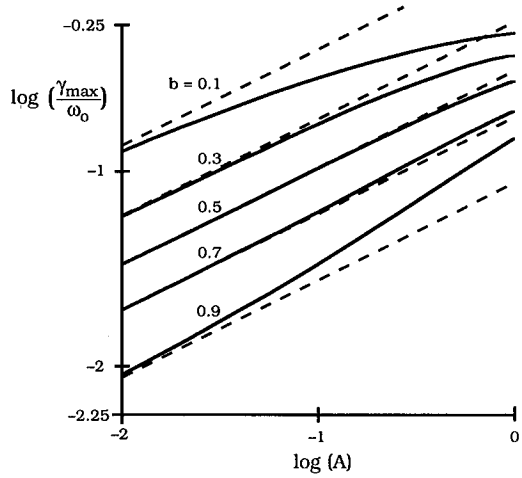

Fig. 3. The maximum growth rate as function of A obtained from approximation (5) (dashed curves) and from the exact roots of (1) (solid curves). Note that the approximation tends to fail as $b \to 0$ and $b \to 1$.

Figure 3 compares approximation (5) with the maximum growth rates obtained by solving (1) numerically; the approximate and exact values are the dashed and solid curves, respectively. Approximation (5) is quite accurate for $0.3 < b < 0.7$, but it fails for small values of b and as $b \to 1$.

Finally, it is useful to note that the two solid lines originating at the origin in Figure 2*a* have slopes which are different from the slopes of the forward sound and forward Alfvén lines in Figure 1. The slope at the origin is

$$s = (x/y)_{(x,y)\to(0,0)}$$

From (1) we have

$$4(s-1)(s-b)(s+b) + A(1-3s) = 0 \tag{7}$$

Taking A to be of the order of ε, we seek solutions of the form

$$s = b + \varepsilon\sigma_1 + \varepsilon^2\sigma_2 + \cdots \tag{8}$$

Equation (7) then yields

$$s_1 = b\left[1 + \frac{A(3b-1)}{8b^2(b-1)} - \frac{A^2(3b-1)(3b^2+1)}{128(b-1)^3b^4} + \cdots\right] \tag{9}$$

Equation (9) represents the fact that the phase speed of a low-frequency sound wave is modified by the presence of the pump Alfvén wave. The series fails when $b \to 0$ or $b \to 1$; in those situations it is no longer possible to think in terms of a sound wave superimposed on the pump wave. We will deal with those situations later. Similarly, for the forward propagating Alfvén wave we take

$$s = 1 + \varepsilon\sigma_1 + \varepsilon^2\sigma_2 + \cdots \tag{10}$$

and we find

$$s_2 = \beta + (1-\beta)\left[1 + \frac{A}{2(1-\beta)^2} - \frac{A^2(1+3\beta)}{8(1-\beta)^4} + \cdots\right] \tag{11}$$

Again, the series fails if $\beta \to 1$.

We consider next an alternate approximation for the case $\beta \approx 1$.

4. Case $\beta \approx 1$

As $\beta \to 1$, the *fs* and *fA* lines in Figure 1 tend to overlap, and their intersection with the $-b$ line occurs at the point (1, 1). We expand (1) around this point, and take

$$x = 1 + dx \tag{12a}$$

$$y = 1 + dy \tag{12b}$$

We again take A to be small and of the order of ε, and we initially take dx and dy to be of the order of $\varepsilon^{1/2}$. However, we now take $|b-1|$ to be of order of $\varepsilon^{1/2}$; the ordering of $|b-1|$ is to some extent arbitrary, but we will find that it leads to an approximation which smoothly merges into our other approximations for $\beta < 1$ and $\beta > 1$. Equation (1) then becomes

$$2(dx+dy)[4(dx-dy)^2 - 4(b-1)(dx-dy) - A]$$
$$+ \{6(dx^2-dy^2)^2 - 2A(2dx^2 + 3dx\,dy + 2dy^2)$$
$$- 2(b-1)(dx^2-dy^2)[2(b-1) + dx + 9\,dy]\}$$
$$+ 0(\varepsilon^{5/2}) = 0 \tag{13}$$

The first term in (13) represents three straight lines. One of these, $dy = -dx$, represents the $-b$ root passing through the point (1, 1). Each of the other two lines has a slope of $+1$, but one line lies above and one line lies below the point (1, 1). We will not write down the equations for these two lines, but we note that they intersect the line $dy = -dx$ at the points

$$dy_\pm = \{-(b-1) \pm [A + (b-1)^2]^{1/2}\}/4$$
$$dx_\pm = -dy_\pm \tag{14}$$

The meaning of (14) will be discussed below.

It will turn out that instability occurs in the vicinity of the intersection corresponding to the plus sign in (14). So we expand (13) around that point, taking

$$dy = dy_+ + dy_2 \tag{15a}$$

$$dx = dx_+ + dx_2 \tag{15b}$$

Thus we are doing a double expansion. We find from inspection of the resulting equation that dx_2 and dy_2 should be of the order of $\varepsilon^{3/4}$. To lowest-order, (13) then yields the approximate dispersion relation

$$8S(dy_2^2 - dx_2^2) - \frac{A}{8}[S-(b-1)]^2 + 0(\varepsilon^{9/4}) = 0 \tag{16}$$

where

$$S \equiv [A + (b-1)^2]^{1/2}$$

According to (16), the maximum growth rate is

$$\frac{\gamma_{\max}}{\omega_0} \approx \frac{A^{1/2}[S-(b-1)]}{8S^{1/2}} \tag{17}$$

Note that $\gamma_{\max} \propto A^{3/4}$ if $|b-1| = 0$, in contrast to the $A^{1/2}$ behavior for the decay instability. (We are unable to offer a physical explanation for the $A^{3/4}$ dependence.) Equation (16) agrees with (5) as $A \to 0$ while $(1-b) > 0$ remains finite, in which case $\gamma_{\max} \propto A^{1/2}$; (16) also agrees with (25) below if $A \to 0$ while $(1-b) < 0$ remains finite, in which case $\gamma_{\max} \propto A^{3/2}$. Equation (16) also shows that the range of unstable wavenumbers is approximately

$$-\frac{\gamma_{\max}}{\omega_0} < y - 1 - dy_+ < \frac{\gamma_{\max}}{\omega_0} \tag{18}$$

Figures 4 and 5 are similar to Figure 2, except that the exact roots of (1) (the solid curves) are compared with approximation (16) (the dashed curves). The center solid circle is the point (1, 1) and the other two solid circles are the points $(1 + dx_\pm, 1 + dy_\pm)$ given by (14). In Figure 4, $A = 0.2$ and $b = 0.9$; in Figure 5, $A = 0.2$ and $b = 1.1$. We see that (16) does a reasonably good job of representing x_r, but only in the vicinity of the instability. Equation (16) can lead to moderate errors in $\gamma_{\max}$, but this is in part due to the large values of A and $|b-1|$ which have been chosen for clarity in Figures 4*a* and 5*a*.

In Figure 6 we compare approximation (17) (the dashed curves) with the exact roots (the solid curves) of (1); we have taken b to vary from 0.8 (top curves) to 1.2 (lower curves) in

steps of 0.1. The approximation is rather robust; for $b = 1$ the approximation and the exact roots are essentially indistinguishable.

Finally, we consider the slopes of the lines originating at the origin in Figures 4*a* and 5*a*. We again use (7) for $s = (x/y)_{(x,y)\to(0,0)}$. With A of the order of ε and $|b - 1|$ of the order of $\varepsilon^{1/2}$, we write

$$s = 1 + \varepsilon^{1/2}\sigma_1 + \varepsilon\sigma_2 + \cdots \tag{19}$$

and (7) then yields

$$s_3 = 1 + \frac{b - 1 - S}{2} + \frac{A}{8} + \cdots \tag{20a}$$

$$s_4 = 1 + \frac{b - 1 + S}{2} + \frac{A}{8} + \cdots \tag{20b}$$

To the order of $\varepsilon^{1/2}$, the intersections of these two lines with the line $y = 2 - x$ (i.e., the $-b$ line in Figure 1) are $y = 1 + dy_\pm$, where $dy_\pm$ is given by (14).

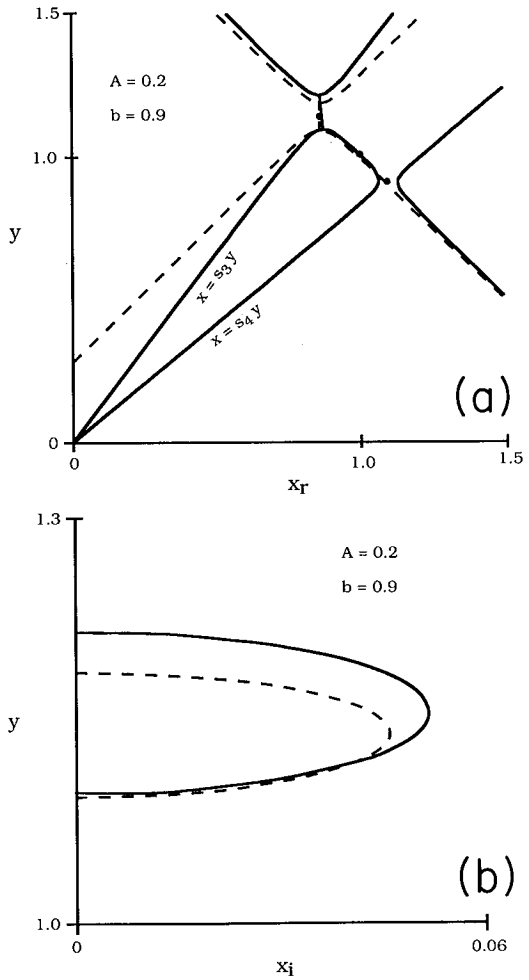

Fig. 4. The (*a*) real and (*b*) imaginary parts of x as functions of y for $A = 0.2$ and $b = 0.9$ ($\beta = 0.81$). The solid curves are from (1) and the dashed curves are from approximation (16). The solid circle in the center is the point (1, 1), and the other solid circles are the points $(1 + dx_\pm, 1 + dy_\pm)$ given by (14).

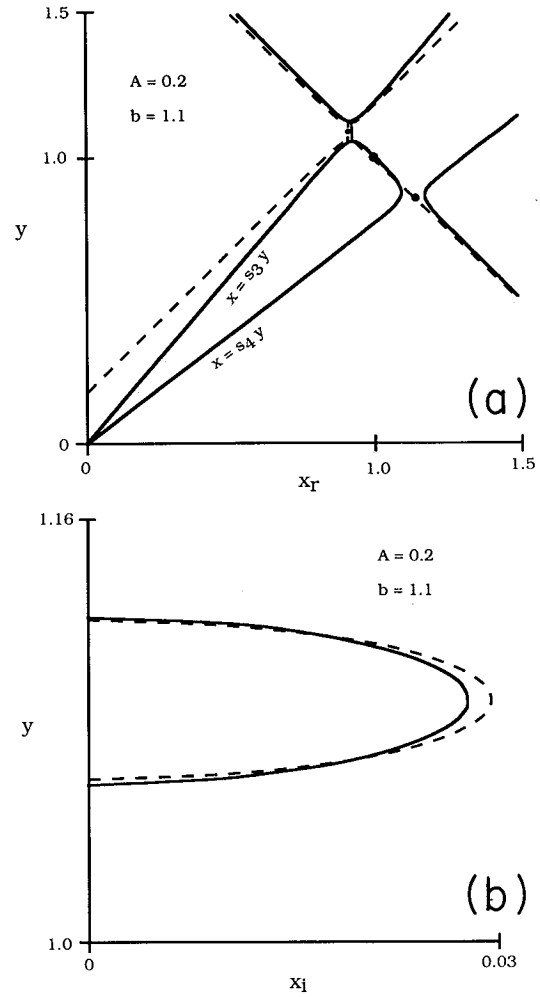

Fig. 5. Same as Figure 4 but $b = 1.1$ ($\beta = 1.21$).

5. Beat Instability: $\beta > 1$

We now turn to the case where $b > 1$, but b is taken to be of order unity. In this case, (9) is valid, and it is again possible to recognize one of the roots of (1) as being essentially a sound wave modified by the presence of the pump wave. However, this sound wave is not involved in the instability, and we no longer have decay of the pump wave into a forward propagating sound wave and a backward propagating Alfvén wave. Instead, the instability involves the other root which originates at the origin, that is, the forward Alfvén root described approximately by (11), as well as the backward Alfvén root. These two roots are produced by the beating of the pump wave (at ω_0, k_0) with the compressional wave (at ω, k) to produce the forward Alfvén wave (at ω_+, k_+) or the backward Alfvén wave (at ω_-, k_-). In this sense the instability should be thought of as a beat instability rather than a decay instability.

We first expand (1) around the point $(x, y) = (1, 1)$ and take

$$x = 1 + dx$$

$$y = 1 + dy$$

Taking A, dx, and dy to be of the order of ε, (1) becomes

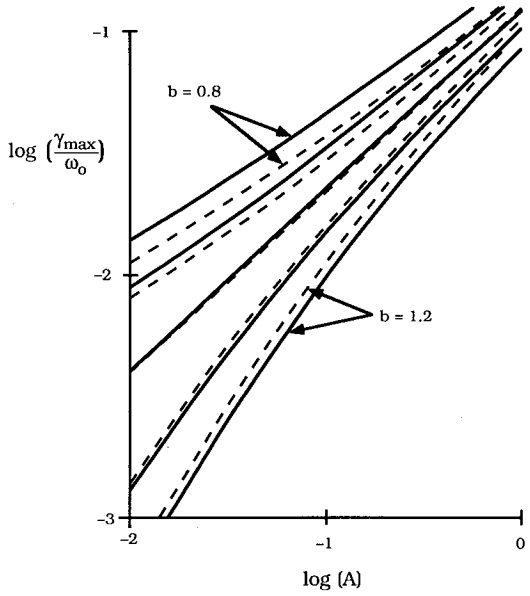

Fig. 6. The maximum growth rate as function of A obtained from approximation (17) (dashed curves) and from the exact roots of (1) (solid curves). The value of b ranges from 0.8 to 1.2 in steps of 0.1. The approximation and the exact values are nearly indistinguishable when $b = 1$ ($\beta = 1$); in this case, $\gamma_{max} \propto A^{3/4}$.

$$-(dx + dy)\{(dy - dx)[4(1 - \beta) + dy(1 - 9\beta) + dx(9 - \beta)] + 2A\} - 2A(2\,dx^2 + 3\,dx\,dy + 2dy^2) + 0(\varepsilon^4) = 0 \quad (21)$$

The first term in (21) is zero when

$$dy = dy_s = \frac{1}{4}\left\{\frac{1 - \beta}{1 + \beta} + \left[\frac{2A}{1 + \beta} + \frac{(1 - \beta)^2}{(1 + \beta)^2}\right]^{1/2}\right\} \quad (22a)$$

$$dx = dx_s = -dy_s \quad (22b)$$

It can be shown that to the order of ε^2 the point $(x, y) = (1 + dx_s, 1 + dy_s)$ is the intersection of the line $x = ys_2$ (with s_2 given by (11)) with the line $y = 2 - x$ (i.e., the $-b$ line in Figure 1).

We again do a double expansion, so (21) is expanded around the point

$$dy = dy_s + dy_2 \quad (23a)$$

$$dx = dx_s + dx_2 \quad (23b)$$

Inspection of (21) then reveals that dx_2 and dy_2 are of the order of $\varepsilon^{3/2}$. To lowest order, (21) then becomes

$$-\frac{A^3 + 32(\beta - 1)^3(dx_2^2 - dy_2^2)}{8(\beta - 1)^2} + 0(\varepsilon^{7/2}) = 0 \quad (24)$$

Equation (24) is our approximate dispersion relation for the instability. According to (24), the maximum growth rate is

$$\frac{\gamma_{max}}{\omega_0} \approx \frac{A^{3/2}}{4\sqrt{2}(\beta - 1)^{3/2}} \quad (25)$$

and the range of unstable wavenumbers is approximately

$$-\frac{A^{3/2}}{4\sqrt{2}(\beta - 1)^{3/2}} < y - 1 - dy_s < \frac{A^{3/2}}{4\sqrt{2}(\beta - 1)^{3/2}} \quad (26)$$

The growth rate declines rapidly as β increases; this reflects the fact that density perturbations are required for the instability, while $\beta \to \infty$ represents the incompressible limit.

Figure 7 again compares the exact roots (the solid curves)

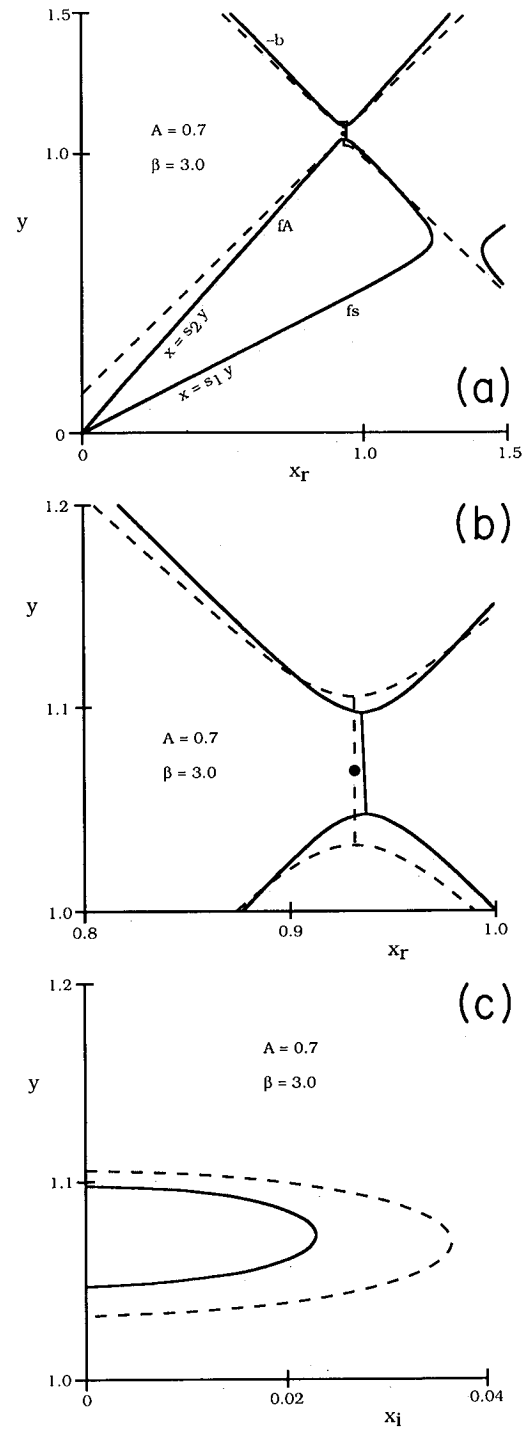

Fig. 7. The (a) and (b) real and (c) imaginary parts of x as functions of y for $A = 0.7$ and $\beta = 3$. The solid curves are from (1), and the dashed curves are from approximation (24). The solid circle is the expansion point given by (22).

with approximation (24) (the dashed curves); we have taken $\beta = 3$ and $A = 0.7$. We have chosen a large value of A for clarity, but Figure 7*c* shows that (24) then leads to a significant overestimate of the growth rate.

Our estimate of γ_{max} is compared with the numerical values in Figure 8; the dashed lines represent (25), and the solid curves give the exact values. As expected, approximation (25) tends to fail as A becomes large, but it becomes an increasingly better approximation as β increases.

6. Case $\beta \approx 0$

The analysis for very small values of β is more involved than the other cases. The numerical roots of (1) are displayed in Figure 9 for the case $A = 0.01$ and $b = 0.03$ ($\beta = 9 \times 10^{-4}$). In this case there is a very broad range of instability, spanning the range $1.7 < y < 3.9$. In fact, the upper limit on the range of instability, y_{max}, approaches infinity as $\beta \to 0$; by taking $x = 0$ in (1) we find

$$y_{max} \approx (4 + A/\beta)^{1/2} \tag{27}$$

We will therefore find it necessary to develop two different expansions to cover the broad range of y.

It should also be noted that the slopes of the two steep lines originating at the origin do not correspond to the speed of sound. We again solve (7), taking A to be of the order of ε, and b to be of the order of $\varepsilon^{1/2}$ (so that β is of the order of ε, as suggested by (27)). With

$$s = \varepsilon^{1/2}\sigma_0 + \varepsilon\sigma_1 + \cdots \tag{28}$$

we obtain

$$s_5 = \pm(\beta + A/4)^{1/2} - A/4 + \cdots \tag{29}$$

Equation (29) remains valid as $\beta \to 0$. To some extent, (29) can be thought of as the dispersion relation for a primarily transverse wave propagating on a coiled spring, the spring being the pump wave; the plasma pressure contributes an additional restoring force and enhances the phase speed. Thus we again encounter a situation where the instability is fundamentally different in nature from the classic decay of a pump wave into forward sound and backward Alfvén waves.

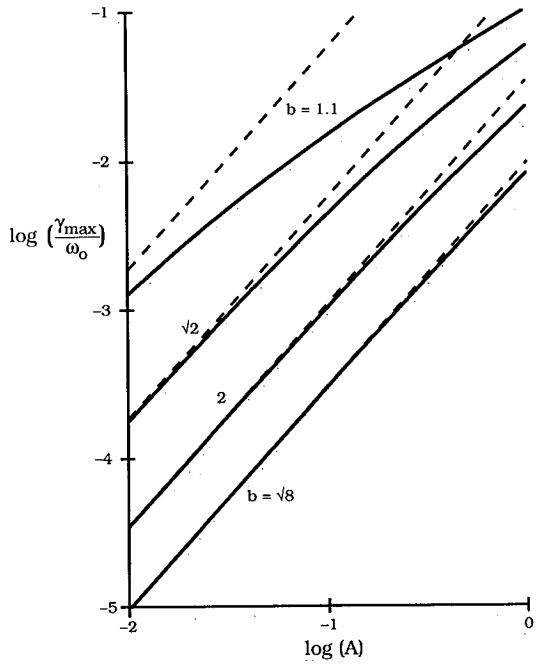

Fig. 8. The maximum growth rate as function of A obtained from approximation (25) (dashed curves) and from (1) (solid curves). The approximation implies $\gamma_{max} \propto A^{3/2}$.

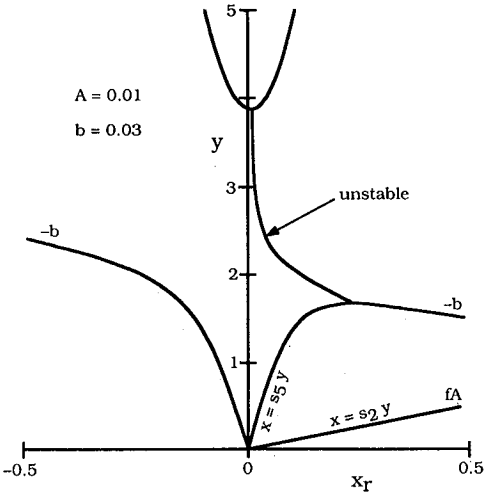

Fig. 9. The roots of (1) for a "low-beta" case, $A = 0.01$ and $b = 0.03$ ($\beta = 9 \times 10^{-4}$). The broad region of instability does not correspond to the interaction of two modes.

We begin by expanding (1) around the point $(x, y) = (0, 2)$, so that

$$x = dx \tag{30a}$$

$$y = 2 + dy \tag{30b}$$

With A and β of order ε we take dx and dy to be of the order of $\varepsilon^{1/3}$; this choice is again dictated by inspection of (1). Equation (1) then becomes

$$-8(A + dy\ dx^2 + dx^3) + 0(\varepsilon^{4/3}) = 0 \tag{31}$$

Equation (31) gives the maximum growth rate when $dy = 0$:

$$\frac{\gamma_{max}}{\omega_0} \approx \frac{3^{1/2}A^{1/3}}{2} \tag{32}$$

In contrast to the cases considered previously, the real and imaginary parts of ω are here comparable.

We now have to use a new expansion if dy is not small. We again take A and β to be of order ε, but we now take dy to be of order unity. If we further take dx to be of order $\varepsilon^{1/2}$, as suggested by (29), then (1) becomes

$$-(2 + dy)\{dx^2\ dy(4 + dy) + (2 + dy)^2 \cdot [A - \beta\ dy(4 + dy)]\} + 0(\varepsilon^{3/2}) = 0 \tag{33a}$$

which has the solution

$$\frac{x}{y} = \pm\left[\beta - \frac{A}{y^2 - 4}\right]^{1/2} \tag{33b}$$

Equation (33*b*) agrees with expression (29) for s_5 a $y \to 0$, and it also agrees with (27) for y_{max}. However, (33) fails (as expected) when $y \to 2$.

Figure 10*a* compares the exact roots of (1) (the solid

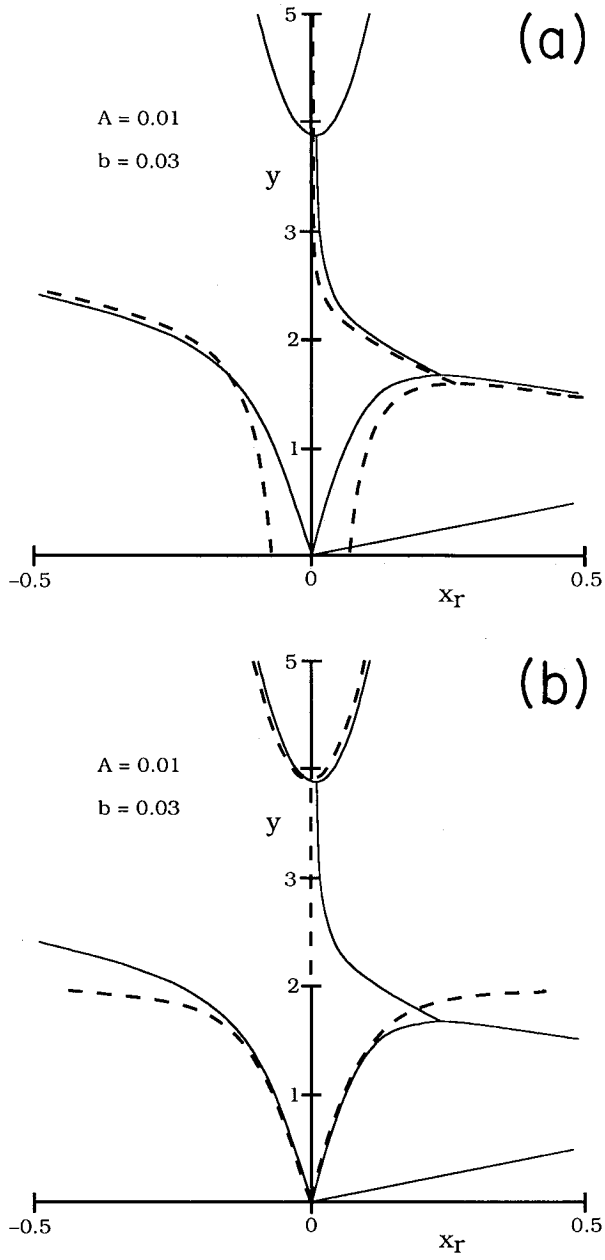

Fig. 10. Same as Figure 9, but the dashed curves are derived from (*a*) approximation (31) and (*b*) approximation (33).

curves) with the roots of the approximate cubic equation (31) (the dashed curves); we have taken $A = 0.01$ and $b = 0.03$. The failure of approximation (31) is evident if $|dy| \gtrsim 0.5$. Note in particular that (31) misses the parabolic behavior at $y \gtrsim 4$, and it fails near the origin. The other approximation, that is, the quadratic (33), is compared with the roots of (1) in Figure 10*b*; again, $A = 0.01$ and $b = 0.03$. We see that (33) succeeds where (31) fails: it correctly represents the behavior near the origin, and it includes the parabolic behavior at $y \gtrsim 4$.

Growth rates derived from approximations (31) (dashes) and (33) (dots) are compared with the exact roots of (1) (solid curve) in Figure 11, for $A = 0.01$ and $b = 0.03$. Equation (31) yields a reasonable approximation to the behavior in the vicinity of maximum growth, while (33) is useful for approximating the decline of the growth rate in the vicinity of y_{max}.

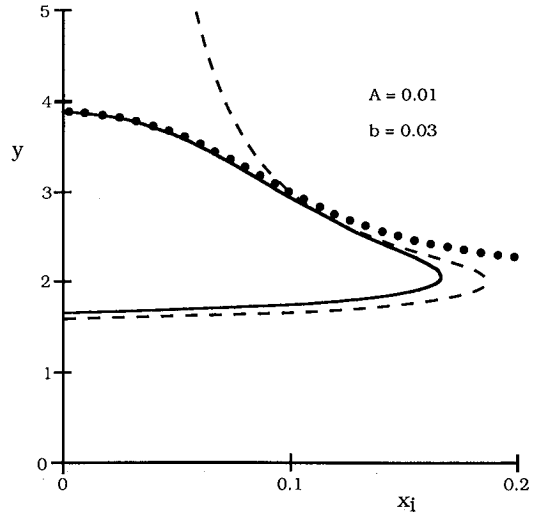

Fig. 11. Growth rates corresponding to Figures 9 and 10. The solid curve is derived from (1), the dashed curve is from approximation (31), and the dotted curve is from approximation (33). The portion of the solid curve which is well-represented by the dots is a nearly purely growing mode.

Note that the growth rate can substantially exceed the real part of the frequency when dy is positive and of order unity, and the instability can be nearly purely growing.

Figure 12 compares the approximation (dashed line) for γ_{max} given by (32) with the roots of (1) (the solid curves) for four values of β. The approximation is useful only for very small values of β.

We have obtained an alternate approximation by taking

$$dx = dx_c + dx'$$

with dx_c of the order of $\varepsilon^{1/3}$ and dx' of the order of $\varepsilon^{2/3}$. With dy of the order of $\varepsilon^{1/3}$ we find that dx_c is given by the cubic equation (31), and

$$dx' = \frac{(16\beta - 3A)\ dy + (16\beta + 5A)\ dx_c}{(8\ dy + 12\ dx_c)\ dx_c} \qquad (34)$$

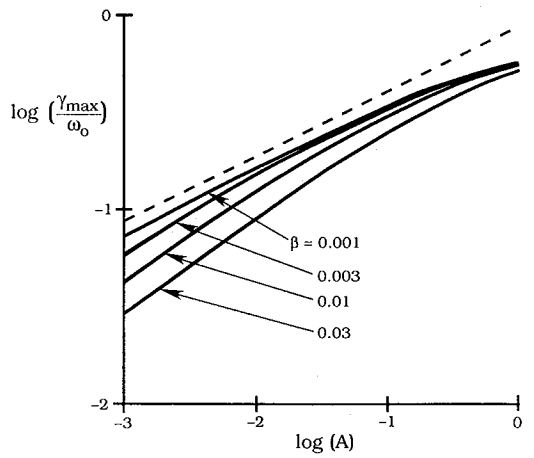

Fig. 12. The maximum growth rate as function of A obtained from approximation (32) (dashed curves) and from (1) (solid curves). The dashed line implies $\gamma_{max} \propto A^{1/3}$.

We can show that the maximum growth rate occurs for a value of dy which is of the order of $A^{2/3}$, so for self-consistency we obtain γ_{max} by taking $dy = 0$ in (31) and (34):

$$\frac{\gamma_{max}}{\omega_0} \approx \frac{3^{1/2}A^{1/3}}{2}\left[1 - \frac{(5 + 16\beta/A)A^{1/3}}{12}\right] \tag{35}$$

Note that (35) will fail if $A^{2/3} \lesssim 4\beta/3$; this is not surprising since our expansion procedure assumed that β and A are both of the order of ε. Figure 13 compares approximation (35) with the exact roots of (1); the approximation is quite accurate over a limited range of A, but the failure of (35) when A becomes smaller than β is evident. If $A \ll \beta$, approximation (5) becomes valid and the instability is then equivalent to the familiar decay instability.

Finally, for completeness we give the result of a higher-order expansion for the case where dy is of order unity. We write

$$dx = dx_q + dx''$$

where dx_q is of the order of $\varepsilon^{1/2}$ and dx'' is of the order of ε. We find that dx_q is given by the quadratic equation (33) and

$$dx'' = \frac{2A(2 + dy)(2 + 4\ dy + dy^2)}{[dy(4 + dy)]^2} \tag{36}$$

It is interesting to note that some of the results of this section are similar to results obtained by *Forslund et al.* [1972] for parametric instabilities of whistler waves. Our (33) is a generalization of their (7), while our (32) is formally similar to their (6), except for different definitions of A.

7. Polarizations

Since some of the instabilities discussed above do not resemble the usual decay instability, it will be useful to learn more about their properties. We will follow the analysis given by *Hollweg et al.* [1993] (hereafter referred to as HEJ). In that paper the ambient magnetic field $\mathbf{B}_0$ was taken to point in the x direction; the pump wave and the unstable waves were also taken to propagate in the x direction. HEJ defined a complex transverse velocity $V_\perp = V_y + iV_z$; similarly, $B_\perp = B_y + iB_z$. The circularly polarized pump wave was written as

$$B_{\perp 0} = \Delta B \exp(ik_0 x - i\omega_0 t)$$

where x here refers to the spatial coordinate and ΔB, k_0, and ω_0 are taken to be real. The transverse velocity fluctuations were taken to have the form

$$\delta V_\perp = v_+ \exp(ik_+ x - i\omega_+ t) + v_- \exp(ik_- x - i\omega_- t) \tag{37}$$

while the longitudinal velocity fluctuations have the form

$$\delta V_x = \mathrm{Re}\,[u \exp(ikx - i\omega t)] \tag{38}$$

HEJ defined $k_+ = k_0 + k$, $k_- = k_0 - k^*$, $\omega_+ = \omega_0 + \omega$, and $\omega_- = \omega_0 - \omega^*$, where the asterisk denotes a complex conjugate.

From (6) and (12) of HEJ we find that the velocity polarizations are given by

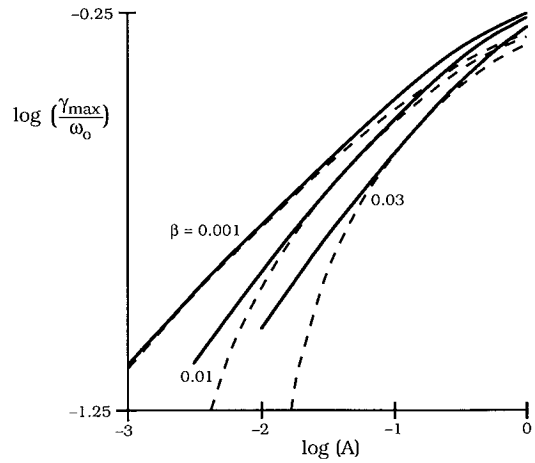

Fig. 13. Same as Figure 12, but the dashed curves represent the alternate approximation (35).

$$\frac{v_+}{u} = -\frac{A^{1/2}}{2}\frac{1}{x_+^2 - y_+^2}\left(x_+ - \frac{yx_+}{x} + y_+^2\right) \tag{39}$$

$$\frac{v_-}{u^*} = -\frac{A^{1/2}}{2}\frac{1}{x_-^2 - y_-^2}\left(x_- - \frac{y^*x_-}{x^*} + y_-^2\right) \tag{40}$$

where $x_+ = 1 + x$, $y_+ = 1 + y$, $x_- = 1 - x^*$, and $y_- = 1 - y^*$ (and x and y now again refer to the normalized frequency and wavenumber used in this paper; i.e., $x = \omega/\omega_0$, $y = k/k_0$). In obtaining (39) and (40) we have restricted the results of HEJ to an electron-proton plasma, and we have eliminated dispersive effects by taking $\omega_c \to \infty$, where ω_c is a cyclotron frequency.

We will be interested in the extent to which the waves are transversely or longitudinally polarized. The degree of transverse polarization is

$$T \equiv \frac{\langle \delta V_y^2 + \delta V_z^2 \rangle}{\langle \delta V_x^2 \rangle} = 2\left[\frac{v_+}{u}\frac{v_+^*}{u^*} + \frac{v_-}{u^*}\frac{v_-^*}{u}\right] \tag{41}$$

where the angle brackets indicate a spatial average. We are also interested in the extent to which the transverse component is dominated by v_+ or v_-. Accordingly, we define the degree of "plus" polarization as

$$P \equiv \frac{v_+ v_+^*}{v_- v_-^*} \tag{42}$$

In Figures 14–19 we use pen thickness to represent the degree of transverse polarization; thus a thick pen is used if the polarization is mainly transverse ($T > 2$), a thin pen is used if the polarization is mainly longitudinal ($T < 0.5$) and a pen of intermediate thickness is used if there is a roughly equal mix of transverse and longitudinal components ($0.5 \le T \le 2$). We use dashing to represent the relative importance of v_+ or v_-; a solid curve represents plus polarization ($P > 2$), a dashed curve represents a roughly equal mix of plus and "minus" polarizations ($0.5 \le P \le 2$), and a gray curve is used to represent minus polarization ($P < 0.5$). To construct Figures 14–19, the exact roots of equation (1) were used.

In Figure 14 we present the familiar decay instability for the same parameters used in Figure 2; i.e., $A = 0.1$ and $b = 1/2$ ($\beta = 1/4$). The forward Alfvén (fA) and backward Alfvén

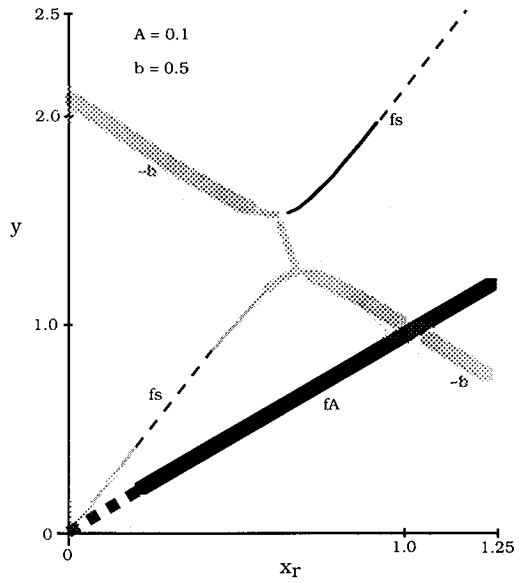

Fig. 14. The dispersion relation, derived from (1), for the same conditions in Figure 2. Line thickness is used to represent the degree of transverse kinetic energy compared to longitudinal kinetic energy; a thick line is used if $T > 2$, a thin line is used if $T < 0.5$, and a line of intermediate thickness is used if $0.5 \leq T \leq 2$. Line density is used to represent the power in v_+ compared to v_-; a solid line is used if $P > 2$, a dashed line is used if $0.5 \leq P \leq 2$, and a gray line is used if $P < 0.5$. The decay instability has a mix of transverse and longitudinal power, and the transverse power is dominated by v_-.

$(-b)$ waves are mainly transverse, and the forward sound (fs) wave is mainly longitudinal, as expected. The forward Alfvén wave is dominated by v_+, except near the origin where there is a tendency for v_+ and v_- to play equal roles. The backward Alfvén wave is dominated by v_-. The wave which we have identified as forward sound is mainly longitudinal, but it does contain some transverse velocity fluctuations, so v_+, $v_- \neq 0$ (see the following paragraph); the relative roles of v_+ and v_- in the forward sound wave exhibit a surprisingly complicated behavior. The instability itself shows a roughly equal mix of transverse and longitudinal components, and the transverse component is dominated by v_-, but the behavior of the polarizations is more complicated in the region around the high-y end of the instability. Figure 14 is consistent with the known result that the decay instability produces a forward propagating sound wave and a backward propagating Alfvén wave given by $\omega_0 - \omega \approx -(k_0 - k)v_A$.

The effect of increased pump amplitude is revealed in Figure 15, which displays the decay instability for $A = 0.5$ and $b = 1/2$ ($\beta = 1/4$). Note that most portions of the curve for the forward sound wave are not thin, indicating that the wave contains a substantial transverse component; in fact, the fs wave is mainly transverse and dominated by v_- near the origin. We believe that there is a simple reason for the sound wave having a substantial transverse component when A is not small: In a low-β plasma the slow mode consists mainly of field-aligned motions which are guided by the strong background magnetic field. However, in this case the background field is at a substantial angle to the x direction, in virtue of the large-amplitude pump. So even field-aligned motions will contain substantial components transverse to the x direction. The instability itself is mainly transverse at its low-y end, and mainly longitudinal at its high-y end; at the high-y end we find the surprising result that the transverse component is no longer dominated by v_-.

The character of the instability is significantly changed if β is large. Figure 16 displays the results for $A = 0.2$ and $b = 0.9$ ($\beta = 0.81$); these are the same parameters used in Figure 4. Note that there are no waves which are predominantly longitudinal. For the values of y giving maximum growth rate the instability contains a mix of transverse and longitudinal components, but in distinct contrast to the decay instability, we now find that the transverse power is domi-

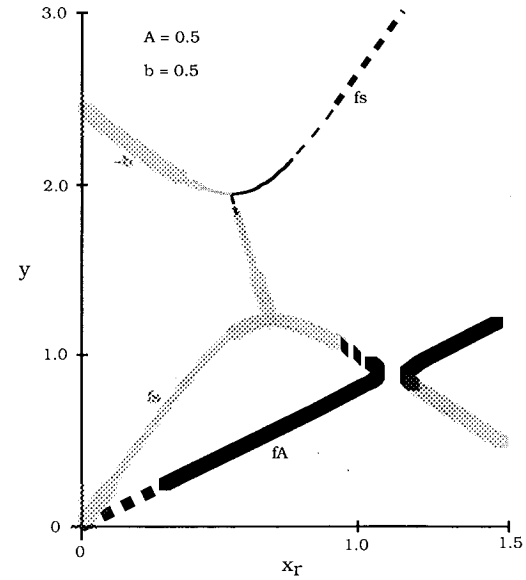

Fig. 15. Same as Figure 14, but for a larger value of A. At the lower values of y the decay instability is mainly transverse, while at the larger values of y the instability is mainly longitudinal and generates a mix of v_- and v_+ transverse components.

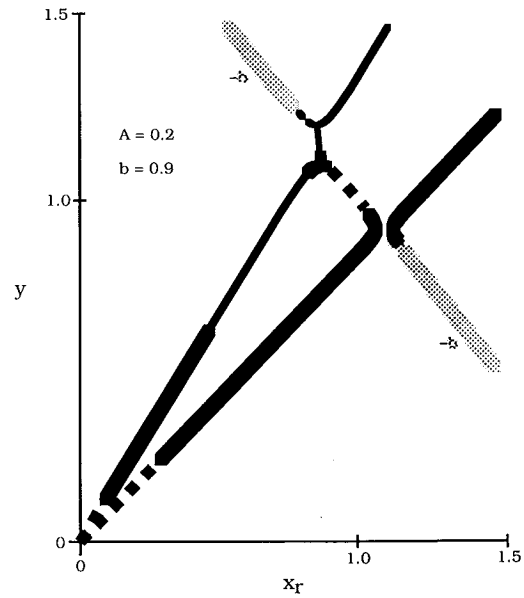

Fig. 16. Same as Figure 14 but for $A = 0.2$ and $b = 0.9$ ($\beta = 0.81$) (cf. Figure 4). In contrast to the usual decay instability the transverse power of the instability is dominated by v_+.

nated by v_+. Thus whereas the decay instability primarily produces a forward propagating sound wave and a backward propagating transverse wave at a low frequency and wavenumber $(\omega_0 - \omega, k_0 - k)$, the instability in Figure 16 produces a forward propagating transverse wave at a high frequency and wavenumber $(\omega_0 + \omega, k_0 + k)$, in addition to the forward propagating longitudinal wave.

If β is increased further, the instability becomes very different from the usual decay instability. Figure 17 is for $A = 0.2$, and $b = 1.1$ ($\beta \approx 1.2$); compare with Figure 5. The instability is now predominantly transverse, and primarily involves a forward propagating wave at$(\omega_0 + \omega, k_0 + k)$.

A similar situation occurs for the parameters used in Figure 7; i.e., $A = 0.7$ and $\beta = 3$. This is the beat instability. The polarizations for this case are displayed in Figure 18. The sound wave ($x \approx by$) appears in the lower right corner of Figure 18 and apparently does not play an important role in the instability, which is in the upper left part of Figure 18. The instability is primarily transverse and involves $(\omega_0 + \omega, k_0 + k)$; this situation has recently been found in numerical MHD simulations by *Umeki and Terasawa* [1992]. This forward propagating transverse wave has a dispersion relation like that of the Alfvén wave but modified by the presence of the pump; i.e.,

$$\frac{\omega_0 + \omega}{k_0 + k} \approx v_A \left[1 + \frac{A}{4(1 - \beta)}\right] \tag{43}$$

which follows from (11) with $k \approx k_0$.

Finally, we consider the low-β case. The polarizations for $A = 0.01$ and $b = 0.03$ (cf. Figures 9 and 10) are displayed in Figure 19. Only at the largest values of y are the waves primarily longitudinal. The instability shows a mix of longitudinal and transverse components, but at $y \approx 2$, where the growth rate is maximal, the transverse component dominates with $T \approx 2$. The transverse component of the instability is dominated by v_-, which is backward propagating.

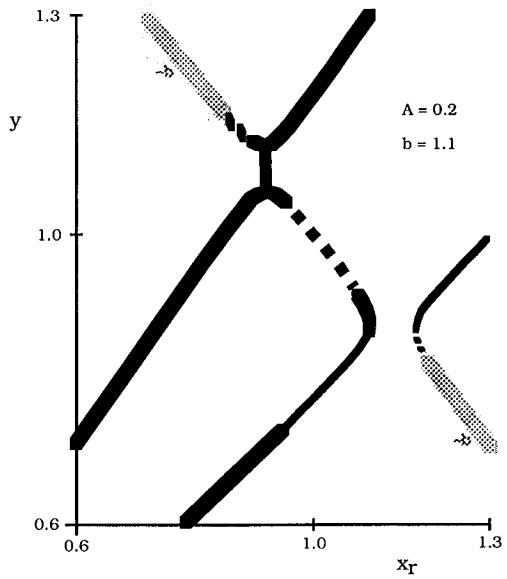

Fig. 17. Same as Figure 14 but for $A = 0.2$ and $b = 1.1$ ($\beta = 1.21$) (cf. Figure 5). In contrast to the usual decay instability the instability here is dominated by transverse power involving v_+.

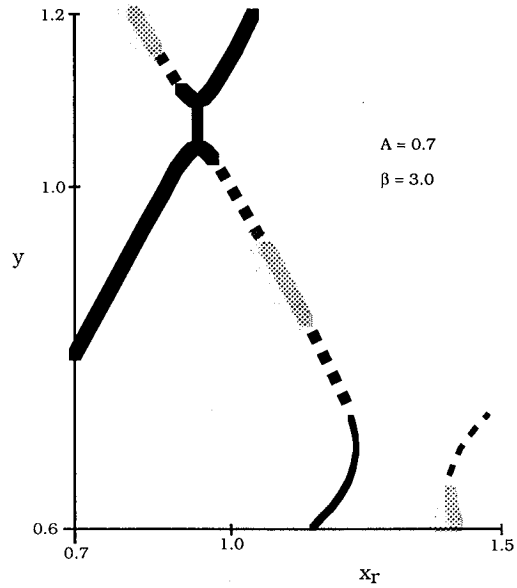

Fig. 18. Same as Figure 14 but for $A = 0.2$ and $\beta = 3$ (cf. Figure 7). The instability here is dominated by transverse power involving v_+.

8. SUMMARY

We have considered the stability of a parallel-propagating circularly polarized Alfvén wave (the "pump wave") to parallel-propagating perturbations. In the dispersionless MHD limit the frequencies $x = \omega/\omega_0$ are related to the wavenumber $y = k/k_0$ by (1), which is well known [e.g., *Derby*, 1978; *Goldstein*, 1978; *Longtin and Sonnerup*, 1986]; here ω_0 and k_0 are the frequency and wavenumber of the pump wave, and ω and k refer to the density perturbations

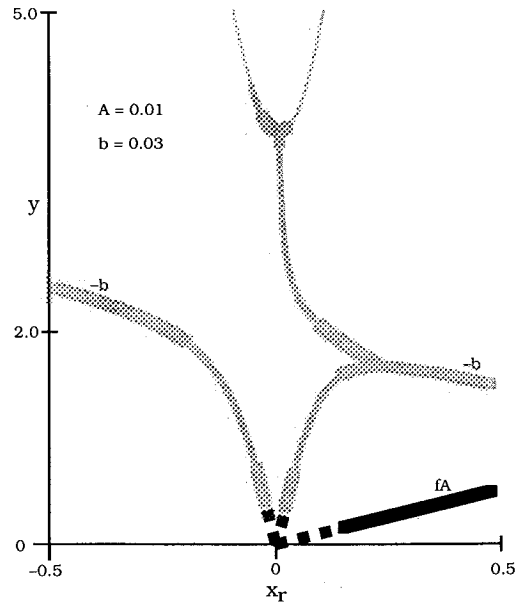

Fig. 19. Same as Figure 14 but for the low-β case $A = 0.01$ and $b = 0.03$ ($\beta = 9 \times 10^{-4}$). Maximum growth occurs at $y \approx 2$; the instability is then primarily transverse and dominated by v_-. At larger values of y (where the instability is nearly purely growing), there is a mix of longitudinal and transverse power, and the transverse component is dominated by v_-.

and related quantities such as the longitudinal velocity perturbations. Our principal goal has been to provide a series of new analytical results based on approximately solving (1) using A as a small expansion parameter; here $A = (\Delta B/B_0)^2$, where B_0 is the strength of the ambient magnetic field and ΔB is the amplitude of the pump.

We find that the plasma β (the square of the ratio of the sound speed to the Alfvén speed) plays a crucial role in determining the nature of the parametric instabilities of the pump. The most familiar instability is the decay instability, in which the pump wave decays into a forward propagating sound wave with the real part of the frequency and the wavenumber given approximately by

$$x_r \approx 2b/(1 + b) \tag{44a}$$

$$y \approx 2/(1 + b) \tag{44b}$$

and into a backward propagating Alfvén wave with lower frequency and wavenumber than the pump, namely, $(1 - x_r)$ and $(1 - y)$, respectively; here $b \equiv \beta^{1/2}$. However, this picture is only valid if $0 < \beta < 1$, but β cannot be too close to either limit. If $\beta \approx 0$ or $\beta \gtrsim 1$, the sound wave is not directly involved in the instability; moreover, if $\beta \gtrsim 1$, the instability is a beat instability.

Consider first the dependence of the maximum growth rate γ_{max} on A. The decay instability has $\gamma_{max} \propto A^{1/2}$ (equation (5), which is a generalization of a result given by *Galeev and Oraevskii* [1963]). However, for $\beta = 0$ we found $\gamma_{max} \propto A^{1/3}$ (equation (32)), for $\beta \approx 1$ we found $\gamma_{max} \propto A^{3/4}$ (equation (17)), while for $\beta \gtrsim 1$ (the beat instability) we found $\gamma_{max} \propto A^{3/2}$ (equation (25)). In addition, for $\beta \approx 0$ the instability having $\gamma_{max} \propto A^{1/3}$ always has comparable real and imaginary parts of ω, and it merges smoothly into a nearly purely growing instability (having a smaller growth rate) with $\gamma_{max} \propto A^{1/2}$ if

$$2 + \frac{4A}{(3A^{2/3} + 16\beta)} \leq y \ll (4 + A/\beta)^{1/2}$$

(the upper limit is obtained from (33) while the lower limit is obtained by equating the growth rates given by (32) and (33)); the A dependence of the nearly purely growing mode is more complicated if y is above this range (equation (33)), while the $A^{1/3}$ dependence takes over if $y \approx 2$.

The fact that the growth rate scales as $A^{3/2}$ if $\beta \gtrsim 1$ means that the growth rate can become very small for small pump amplitudes, $A \ll 1$. Thus the modulational instability, which has a growth rate which scales as A [*Longtin and Sonnerup*, 1986, Equation (29)], could be the dominant instability if A is small.

The instabilities do not always have the physical characteristics associated with the usual decay instability, namely, decay of the pump into a forward propagating sound wave, and into a backward propagating transverse wave involving ω_- and k_-, which we have called the $-b$ wave. This is clearly the case when $\beta \approx 0$. According to (31), the maximum growth rate occurs for

$$x_r \approx A^{1/3}/2 \tag{45a}$$

$$y \approx 2 \tag{45b}$$

which does not agree with (44a) for the usual decay instability. Indeed, there can be an instability even when $\beta = 0$, and there is no sound wave at all. The net result is that the unstable wave is primarily transverse and backward propagating, and primarily involves $\omega_- \approx \omega_0$ and $k_- \approx -k_0$. The nearly purely growing mode which exists when $\beta \approx 0$ is more difficult to characterize. Its transverse component is dominated by $\omega_- \approx \omega_0$ and $k_- < -k_0$, so its propagation speed is less than the Alfvén speed. Moreover, the nearly purely growing mode contains a significant longitudinal component which can be dominant at the larger values of y if $\beta \ll A$. The nearly purely growing instability is not a decay instability.

Consider next the other extreme where β is large, which was examined in section 5. We have suggested that this is best thought of as a beat instability. In this case too the sound wave is not involved in the instability. Instead, the instability primarily produces a forward-propagating transverse wave involving $\omega_+ \approx 2\omega_0$ and $k_+ \approx 2k_0$.

The nature of the instability is more complex if $\beta \approx 1$ (section 4). The transverse component of the unstable wave is forward-propagating and dominated by $\omega_+ \approx 2\omega_0$ and $k_+ \approx 2k_0$.

However, our discussion has omitted two important physical effects, namely, Landau and transit time damping, which will be present in a nearly collisionless plasma such as the solar wind. (We also omit cyclotron damping. This is consistent with a discussion which is based on (1), which is valid only for frequencies well below the ion cyclotron frequency.) Consider first the usual decay instability, for $0 < \beta < 1$. The instability produces a sound wave, which is subject to strong Landau damping unless the electron-ion temperature ratio is large; i.e., $T_e/T_i \gg 1$. This condition is probably not fulfilled in the solar wind; indeed, $T_e/T_i < 1$ in high-speed solar wind streams at 1 AU [e.g., *Feldman et al.*, 1976]. Landau damping will reduce the growth rate, as has been shown by *Inhester* [1990], who applied a drift-kinetic treatment to the decay instability (thus Inhester's method also does not assess the role of cyclotron damping). Inhester found that collisionless damping reduces the growth rate by a factor of 2–3 even when $T_e/T_i \approx 5$; larger values of T_e/T_i have a smaller effect on the growth rate, as expected. If $T_e/T_i \approx 1$, the decay instability is no longer recognizable; there instead appears a kinetic instability of a negative energy wave, which, like the decay instability, produces a backward propagating Alfvén wave. Inhester also found that the damping increases the range of k for which the pump is unstable. Thus our analysis yields an overestimate of the growth rate, and an underestimate of the range of unstable wavenumbers. However, it is noteworthy that in spite of very strong damping of the sound wave, instability is not suppressed. This was observed also by *Terasawa et al.* [1986], who investigated the decay instability using a hybrid code, which automatically includes ion Landau and transit time damping. Their Table 2 compares the simulated growth rates for the decay instability with the analytically predicted growth rates for the dissipationless system. Even though $T_e = T_i$ in the simulations, the growth rates are found to be no smaller than approximately two thirds of the predicted growth rates. It would thus appear that Inhester's analysis overestimates the effects of Landau damping; it is not clear why this is the case.

However, we still have to consider to what extent the parametric dependences of γ_{max} given by (5) remain valid in the presence of damping. Table 2 of Terasawa et al. shows

that the simulated growth rate scales roughly as $A^{1/2}$, but only two runs are available for this comparison, and those runs are for a pump frequency which is sufficiently high to bring ion cyclotron effects into play. The β dependence of γ_{max} is shown in Inhester's Figure 2; the growth rate seems to decrease with increasing β somewhat faster than predicted by our (5).

We also call attention to the hybrid simulations of *Machida et al.* [1987]. They were primarily interested in the evolution of an amplitude-modulated Alfvén wave. Their simulations contain the decay instability, but detailed comparisons with the analysis of this paper are not possible. However, Machida et al. make the interesting observation that amplitude modulation significantly increases the rate at which pump wave energy is converted into heat. Fluid simulations by *Hoshino and Goldstein* [1989] and *Umeki and Terasawa* [1992] include dissipation due to viscosity and electrical resistivity, but these effects are a poor representation of collisionless damping, especially since they directly affect all velocity components, whereas Landau and transit time damping directly affect only the parallel velocity [*Spangler*, 1989, 1990].

We are not aware of any studies which assess the effects of collisionless damping for the other cases considered in this paper, namely, $\beta \approx 0$ or $\beta \gtrsim 1$. If $\beta \approx 0$, the unstable density fluctuations propagate faster than the sound speed, and the Landau damping will be reduced; indeed, there can be instability even when $\beta = 0$, in which case there is no Landau or transit time damping at all. If $\beta \gtrsim 1$, the sound wave is not involved in the instability, and the instability generates primarily a transverse wave which is not subject to Landau damping. It is tempting to speculate that Landau damping may be less important in this case, bt it should be realized that density fluctuations do play an essential role in generating even this instability. However, we must be cautioned by the lower panels in Inhester's Figure 2, which convey the same information about the dispersion relation as our plots of y versus x_r (although Inhester does not display the root which has $x_r > y$, or the root which corresponds to $x = y$ in equation (1)). For $T_e/T_i = 9$ and for $\beta \lesssim 0.5$, Inhester's plots show features which closely resemble the "gaps" which represent instability in our y-x_r plots. However, for larger values of β, Inhester's solutions for the dispersion relation do not resemble ours; for example, the gap appearing near the top of our Figure 4*a* does not appear in the third of the lower panels of Inhester's Figure 2, even though the parameters are nearly the same. The possible implication is that our results for $\beta \approx 1$ or for $\beta \gtrsim 1$ have no application to a collisionless system such as the solar wind. Since the solar wind can have $\beta \gtrsim 1$ at 1 AU, it would seem that further work on parametric instabilities in this parameter regime is warranted. No hybrid simulations have been presented for this case. Although Inhester's expressions could be numerically evaluated for $\beta \gtrsim 1$, he has not done so.

The importance of kinetic effects has been emphasized also by *Mjølhus and Wyller* [1988] and by *Spangler* [1989, 1990] in a related context. They were primarily interested in the longitudinal velocity and density perturbations driven by the Alfvén wave ponderomotive force, with applications to the modulational instability and the nonlinear wave equation. They found that kinetic theory yields results which are substantially different from the fluid analysis when $\beta \gtrsim 1$.

The properties of the various instabilities discussed in this paper have several physical implications, but, as discussed in the preceding paragraphs, our results for $\beta \approx 1$ or for $\beta \gtrsim 1$ have to be viewed with caution. Parametric instabilities have been discussed as possibly playing a role in MHD turbulence. *Dobrowolny et al.* [1980] have shown that incompressible turbulence occurs through the nonlinear interaction of oppositely propagating Alfvén waves, and many other discussions of turbulence have been based on this notion [e.g., *Tu et al.*, 1984, 1987; *Marsch*, 1991]. *Chin and Wentzel* [1972] have suggested that a cascade can develop if a newly generated backward-propagating Alfvén wave in turn decays into a forward propagating Alfvén wave, and so on. The decay instability for $0 < \beta < 1$ (section 3) may be an important part of these processes, since it generates backward propagating Alfvén waves. The nearly purely growing mode which occurs when $\beta \approx 0$, and the rapidly growing ($\gamma_{max} \propto A^{1/3}$) mode which occurs when $\beta \approx 0$ and $y \approx 2$, can also generate backward propagating transverse waves, but the phase speeds of these modes can be substantially less than v_A, and they should not be identified with Alfvén waves. In any event, both the turbulence and cascade pictures will depend on the growth rates of the instabilities which lead to the new waves, and on the physical nature of the new waves. In this regard we point out that the unusual situations which occur when $\beta \approx 0$, namely, the nearly purely growing mode and the mode with $\gamma_{max} \propto A^{1/3}$, have not been considered in the turbulence or cascade scenarios. For example, *Chin and Wentzel* [1972] envision a cascade of wave energy to ever smaller wavenumbers, but the nearly purely growing mode produces transverse waves with wavenumbers greater than that of the pump.

If $\beta \gtrsim 1$ the situation is quite different, since the instabilities can generate forward-propagating transverse waves with both frequency and wavenumber which are approximately twice the pump values. (This has been found in numerical simulations by *Umeki and Terasawa* [1992].) This allows energy to be transferred to high wavenumbers directly, rather than by a cascade. (However, the fact that the growth rates scale as $A^{3/4}$ ($\beta \approx 1$) or $A^{3/2}$ ($\beta > 1$) means that a higher-order analysis than that of *Chin and Wentzel* [1972] will be required.) The case $\beta \gtrsim 1$ may be important in interpreting solar wind data, since that is frequently the case in high-speed solar wind streams. The different character of the instabilities when $\beta \gtrsim 1$ seems to have been overlooked. For example, *Inhester* [1990, p. 10,533] incorrectly states that "coupling becomes impossible [when] the ion sound velocity exceeds the Alfvén velocity." *Chin and Wentzel* [1972] state that the coupling coefficient vanishes for decay into two Alfvén waves, but this is essentially the situation which occurs when $\beta \gtrsim 1$ (Figures 16–18). *Hoshino and Goldstein* [1989, p. 1407] incorrectly assert that "left-hand polarized Alfvén waves in high beta plasmas ($\beta > 1$) are stable against parametric instabilities"; we have verified that the beat instability discussed in section 5 exists even when ion-cyclotron effects are taken into account.

One of the questions which has been addressed in terms of decay instabilities is the origin of solar wind fluctuations which, when described in terms of Elsässer variables, correspond to Alfvén waves with a sense of propagation toward the sun [e.g., *Marsch and Tu*, 1990; *Roberts et al.*, 1987], even when the solar wind fluctuations are dominated by outward propagating waves. *Inhester* [1990] suggests that

decay instabilities provide a natural explanation for the inward traveling waves. However, this picture does not work as well if $\beta \gtrsim 1$, since the instability then leads primarily to fluctuations propagating in the same sense as the pump. For example, the fastest growing wave in Figure 16 ($\beta = 0.81$) has $P \approx 3$, while the fastest growing wave in Figure 17 ($\beta = 1.21$) has $P \approx 12$; larger values of β lead to still larger values of P. (An alternative point of view has been presented by *Lou* [1993], who explored the possibility that non-WKB effects can explain the presence of both Elsässer variables in the solar wind wave spectrum. However, this mechanism only works at very low frequencies and does not seem capable of explaining the presence of both Elsässer variables throughout the entire range of observed frequencies. See also *Hollweg* [1990].)

However, the instabilities which occur when $\beta \gtrsim 1$ may help to explain the observation that solar wind fluctuations tend to have more magnetic energy than kinetic energy. The transverse waves generated in Figures 16–18 are mainly at frequencies and wavenumbers $\omega_0 + \omega$ and $k_0 + k$, respectively, but

$$\frac{\omega_0 + \omega}{k_0 + k} < v_A \tag{46}$$

A simple exercise using Faraday's law and $\mathbf{E} \times \mathbf{B}$ drifts shows that inequality (46) implies an excess of magnetic energy. A similar remark can be applied to the nearly purely growing mode and to the mode having $\gamma_{\max} \propto A^{1/3}$ which exist when $\beta \approx 0$; the transverse components of these modes are dominated by ω_- and k_-, but $|(\omega_0 - \omega)/(k_0 - k)| < v_A$.

Finally, we have to evaluate whether the instabilities can grow fast enough to develop in the solar wind as it flows from the Sun to ~1 AU, where turbulence has developed and some backward propagating waves are present [*Roberts et al.*, 1987]. We will assume that $\beta = 1$ throughout most of the solar wind. Equation (17) then gives

$$\gamma_{\max} \approx A^{3/4}\omega_0/8 \tag{47}$$

In the solar wind a typical value for A is $A \approx 1/2$. Most power is at periods of several hours in the inertial frame, or at several tens of hours in the solar wind frame for an Alfvén Mach number of 10; we will adopt a plasma frame period of 1 day as representative. The e-folding time is then 2.1 days, according to (47). However, since collisional effects reduce the growth rate, this is an underestimate, by a factor between 1.5 [*Terasawa et al.*, 1986] and 3 [*Inhester*, 1990]. Moreover, the solar wind power spectrum is not monochromatic as has been assumed here. *Umeki and Terasawa* [1992] found that the broadband nature of the pump wave does not change the physical nature of the instabilities, but their simulations suggest that the growth time should be increased by another factor of 3–5 for a power law power spectrum such as is observed in the solar wind. Thus the growth time becomes 10–30 days, which is considerably longer than the 4 days required for the solar wind to traverse 1 AU. Higher-frequency waves will grow faster in virtue of the ω_0 dependence in (47), but there is less power at higher frequencies so A is smaller; in fact the $A^{3/4}$ dependence overwhelms the ω_0 dependence for solar wind spectra which vary as $k_0^{-3/2}$ or $k_0^{-5/3}$. It thus seems unlikely that the instabilities discussed in this paper play a significant role in the solar wind inside 1 AU.

Acknowledgments. The authors are grateful to M. A. Lee and P. A. Isenberg for helpful discussions. We have also benefitted greatly from S. Spangler's comments on an earlier version of this manuscript. This work has been supported in part by the NASA Space Physics Theory Program under grant NAG5-1479 and in part by JPL contract 955461, to the University of New Hampshire.

The Editor thanks S. Spangler and A. A. Galeev for their assistance in evaluating this paper.

REFERENCES

Abraham-Shrauner, B., and W. C. Feldman, Nonlinear Alfvén waves in high-speed solar wind streams, *J. Geophys. Res.*, *82*, 618, 1977.

Agim, Z., M. L. Goldstein, and S. Ghosh, Magnetic and density fluctuation spectra from parametric instabilities of large-amplitude Alfvén waves, *Eos Trans. AGU*, *74*, 240, 1993.

Barnes, A., and J. V. Hollweg, Large-amplitude hydromagnetic waves, *J. Geophys. Res.*, *79*, 2302, 1974.

Barnes, A., and G. C. J. Suffolk, Relativistic kinetic theory of the large-amplitude transverse Alfvén wave, *J. Plasma Phys.*, *5*, 315, 1971.

Chin, Y.-C., and D. G. Wentzel, Nonlinear dissipation of Alfvén waves, *Astrophys. Space Sci.*, *16*, 465, 1972.

Derby, N. F. J., Modulational instability of finite amplitude circularly polarized Alfvén waves, *Astrophys. J.*, *224*, 1013, 1978.

Dobrowolny, M., A. Mangeney, and P. Veltri, Properties of magnetohydrodynamic turbulence in the solar wind, *Astron. Astrophys.*, *83*, 26, 1980.

Feldman, W. C., J. R. Asbridge, S. J. Bame, and J. T. Gosling, High-speed solar wind flow parameters at 1 AU, *J. Geophys. Res.*, *81*, 5054, 1976.

Forslund, D. W., J. M. Kindel, and E. L. Lindman, Parametric excitation of electromagnetic waves, *Phys. Rev. Lett.*, *29*, 249, 1972.

Galeev, A. A., and V. N. Oraevskii, The stability of Alfvén waves, *Sov. Phys. Dokl.*, Engl. Transl., *7*, 988, 1963.

Ghosh, S., and M. L. Goldstein, Turbulent evolution of the parametric instabilities of a large-amplitude circularly-polarized Alfvén wave, *Eos Trans. AGU*, *74*, 240, 1993.

Ghosh, S., A. F. Viñas, and M. L. Goldstein, Parametric instabilities of a large-amplitude circularly-polarized Alfvén wave: Linear growth in two-dimensional geometries, *J. Geophys. Res.*, *98*, 15,561, 1993.

Goldstein, M. L., An instability of finite-amplitude circularly polarized Alfvén waves, *Astrophys. J.*, *219*, 700, 1978.

Hollweg, J. V., On WKB expansions for Alfvén waves in the solar wind, *J. Geophys. Res.*, *95*, 14,873, 1990.

Hollweg, J. V., R. Esser, and V. Jayanti, Modulational and decay instability of Alfvén waves: effects of streaming He++, *J. Geophys. Res.*, *98*, 3491, 1993.

Hoshino, M., and M. L. Goldstein, Time evolution from linear to nonlinear stages in magnetohydrodynamic parametric instabilities, *Phys. Fluids B*, *1*, 1405, 1989.

Inhester, B., A drift-kinetic treatment of the parametric decay of large-amplitude Alfvén waves, *J. Geophys. Res.*, *95*, 10,525, 1990.

Jayanti, V., and J. V. Hollweg, On the dispersion relations for parametric instabilities of parallel-propagating Alfvén waves, *J. Geophys. Res.*, *98*, 13,247, 1993.

Longtin, M., and B. U. Ö. Sonerrup, Modulational instability of circularly polarized Alfvén waves, *J. Geophys. Res.*, *91*, 6816, 1986.

Lou, Y.-Q., Propagation of three-dimensional Alfvén waves and its nonlinear effects in the solar wind, *J. Geophys. Res.*, *98*, 3563, 1993.

Machida, S., S. R. Spangler, and C. K. Goertz, Simulation of amplitude-modulated circularly polarized Alfvén waves for beta less than one, *J. Geophys. Res.*, *92*, 7413, 1987.

Marsch, E., MHD turbulence in the solar wind, in *Physics of the Inner Heliosphere*, edited by R. Schwenn and E. Marsch, p. 159, Springer-Verlag, New York, 1991.

Marsch, E., and C.-Y. Tu, On the radial evolution of MHD turbulence in the inner heliosphere, *J. Geophys. Res.*, *95*, 8211, 1990.

Mjølhus, E., and J. Wyller, Nonlinear Alfvén waves in a finite-beta plasma, *J. Plasma Phys.*, *40*, 299, 1988.

Roberts, D. A., M. L. Goldstein, L. W. Klein, and W. H. Matthaeus, Origin and evolution of fluctuations in the solar wind: Helios observations and Helios-Voyager comparisons, *J. Geophys. Res.*, *92*, 12,023, 1987.

Sagdeev, R. Z., and A. A. Galeev, *Nonlinear Plasma Theory*, W. A. Benjamin, Reading, Mass., 1969.

Sakai, J.-I., and B. U. Ö. Sonnerup, Modulational instability of finite amplitude dispersive Alfvén waves, *J. Geophys. Res.*, *88*, 9069, 1983.

Spangler, S. R., Kinetic effects of Alfvén wave nonlinearity, I, Ponderomotive density fluctuations, *Phys. Fluids B*, *1*, 1738, 1989.

Spangler, S. R., Kinetic effects on Alfvén wave nonlinearity, II, The modified nonlinear wave equation, *Phys. Fluids B*, *2*, 407, 1990.

Spangler, S. R., The evolution of large-amplitude MHD waves near quasi-parallel shocks in the solar wind, in *Solar Wind Seven*, edited by E. Marsch and R. Schwenn, p. 539, Pergamon, New York, 1992.

Terasawa, T., M. Hoshino, J. Sakai, and T. Hada, Decay instability of finite-amplitude circularly polarized Alfvén waves: A numerical simulation of stimulated Brillouin scattering, *J. Geophys. Res.*, *91*, 4171, 1986.

Tu, C.-Y., A solar wind model with the power spectrum of Alfvénic fluctuations, *Sol. Phys.*, *109*, 149, 1987.

Tu, C.-Y., Z.-Y. Pu, and F.-S. Wei, The power spectrum of interplanetary Alfvénic fluctuations: Derivation of the governing equation and its solution, *J. Geophys. Res.*, *89*, 9695, 1984.

Umeki, H., and T. Terasawa, Decay instability of incoherent Alfvén waves in the solar wind, *J. Geophys. Res.*, *97*, 3113, 1992.

Viñas, A. F., and M. L. Goldstein, Parametric instabilities of circularly polarized, large amplitude, dispersive Alfvén waves: Excitation of obliquely propagating daughter and sideband waves, *J. Plasma Phys.*, *46*, 129, 1991.

Wong, H. K., and M. L. Goldstein, Parametric instabilities of circularly polarized Alfvén waves including dispersion, *J. Geophys. Res.*, *91*, 5617, 1986.

J. V. Hollweg and V. Jayanti, Physics Department and Institute for the Study of Earth, Oceans and Space, Space Science Center, University of New Hampshire, Durham, NH 03824.

(Received February 16, 1993;
revised July 23, 1993;
accepted July 29, 1993.)